Space Sci Rev (2009) 143: 21–30
DOI 10.1007/s11214-008-9369-5

Constraints on the Structure of the Heliospheric Interface Based on Lyα Absorption Spectra

Brian E. Wood · Vladislav V. Izmodenov · Yury G. Malama

Received: 11 February 2008 / Accepted: 22 April 2008 / Published online: 21 May 2008

Abstract Spectroscopic observations of the hydrogen Lyα lines from nearby stars taken by the *Hubble Space Telescope* (HST) sometimes show absorption signatures from the heliosphere. This absorption is a unique diagnostic of material in the outermost parts of our heliosphere. We summarize how the HST data have been used to test various models of the heliosphere, particularly new 3-dimensional MHD models that have recently become available. We also focus on new detections of heliospheric absorption in very downwind directions, which can only be modeled using heliospheric model codes with extended grids in the downwind direction. We illustrate a couple attempts to reproduce this absorption using a couple of these extended tail models.

Keywords Solar wind · Interstellar medium · Heliosphere · Ultraviolet spectroscopy

1 Introduction

Ever since the first detection of Lyα absorption from the outer heliosphere in 1996 (Linsky and Wood 1996), the absorption has been used to test models of the heliosphere. The absorption comes from hot hydrogen that permeates the heliosphere due to charge exchange processes that occur during the collision of the solar wind and ISM. Detection of the absorption requires high resolution UV spectroscopy, and the only instruments capable of such observations are spectrometers on board the *Hubble Space Telescope* (HST); first the Goddard

B.E. Wood (✉)
JILA, University of Colorado, 440 UCB, Boulder, CO 80309-0440, USA
e-mail: woodb@colorado.edu

V.V. Izmodenov
Dept. of Aeromechanics and Gas Dynamics, Lomonosov Moscow State University, Moscow 119899, Russia
e-mail: izmod@ipmnet.ru

V.V. Izmodenov · Y.G. Malama
Space Research Institute (IKI), Russian Academy of Science, and Institute for Problems in Mechanics, Moscow 117526, Russia

High Resolution Spectrograph (GHRS) and then its 1997 replacement the Space Telescope Imaging Spectrograph (STIS), which unfortunately has been inoperable since August 2004.

The Lyα absorption has confirmed the existence of the "hydrogen wall" predicted by models to exist between the heliopause and bow shock (Baranov et al. 1991). Attempts have been made to use the absorption to constrain ISM properties around the Sun, but with limited success due to model dependence and the sensitivity of the absorption to too many ISM parameters (Wood et al. 2000, 2007a; Izmodenov et al. 2002). Finally, analogous astrospheric absorption detected in the HST spectra have been used to study the solar-like winds of nearby stars and determine how the properties of such winds vary with stellar age and activity (Wood et al. 2005a).

2 The Heliospheric Absorption Detections

Only a small fraction of the Lyα spectra of nearby stars in the HST archive show direct evidence of heliospheric absorption (Wood et al. 2005b). There are two primary factors that determine whether an observed line of sight will have a detectable heliospheric signal. One is the ISM hydrogen column density. Detecting heliospheric absorption requires that the absorption is separable from interstellar absorption. The higher the interstellar H column density, the broader the interstellar absorption, and the more likely that the ISM absorption will hide any heliospheric absorption.

The second factor is the direction of the line of sight with respect to the orientation of the heliosphere. This is quantified by the angle θ between the line of sight and the upwind direction of the ISM flow seen by the Sun, so $\theta = 0°$ is upwind and $\theta = 180°$ is downwind. Figure 1 plots the logarithmic interstellar H column density versus θ for all HST-observed lines of sight, with the boxes being lines of sight with detected heliospheric absorption and the diamonds being nondetections. As expected, the detections tend to have low ISM columns. It is also clearly easier to detect heliospheric absorption in upwind directions than in downwind directions. This is due to the stronger deceleration of heliospheric H in upwind directions, which helps to shift the heliospheric absorption away from the ISM absorption, making it easier to detect.

Most of the absorption detections are in directions where the hydrogen wall dominates the absorption, meaning the absorption is a diagnostic of neutral H properties in between

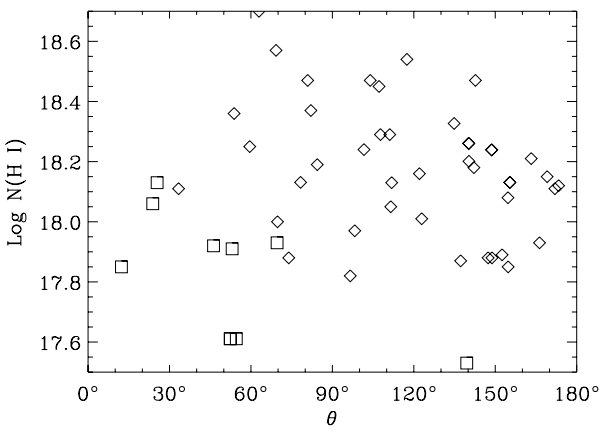

Fig. 1 The ISM H I column densities measured for all HST-observed lines of sight are plotted versus the angle of the lines of sight relative to the upwind direction of the ISM flow seen by the Sun. The *boxes* and *diamonds* indicate lines of sight that yield detections and nondetections of heliospheric absorption, respectively. From Wood et al. (2005b)

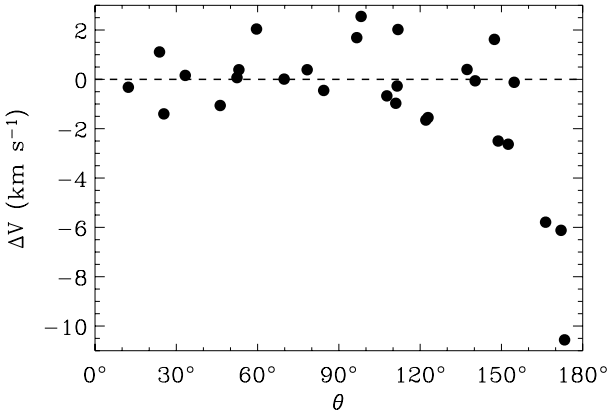

Fig. 2 Velocity difference between the bisectors of stellar Lyα lines and the stellar rest frame plotted as a function of θ, the angle between the line of sight and the ISM flow vector. The Lyα profiles of the most downwind lines of sight ($\theta > 160°$) are systematically blueshifted with respect to the stellar rest frame, suggesting the presence of heliosheath absorption. From Wood et al. (2007b)

the heliopause and bow shock. However, very downwind lines of sight with extended path lengths through the heliotail can potentially be dominated by absorption from heliosheath neutrals, neutrals formed by charge exchange in the inner heliosheath between the termination shock and heliopause. There is only one truly downwind heliospheric absorption detection in Fig. 1 where heliosheath absorption will dominate. The heliosheath absorption is much broader than the hydrogen wall absorption, but is also much shallower, which makes it harder to detect.

However, a less direct method of detecting heliosheath absorption has recently been devised (Wood et al. 2007b). The broad, shallow heliosheath absorption will absorb some of the flux from the red side of the observed stellar Lyα emission line. Therefore, the heliosheath absorption will cause the wings of the stellar emission line to be blueshifted relative to their original centroid, which would correspond to the stellar radial velocity. Figure 2 plots the velocity shifts of reconstructed stellar Lyα profiles as a function of θ. In most directions the profiles are within 2 km s^{-1} of the stellar radial velocity. But not in the most downwind directions with $\theta > 160°$. For the three lines of sight within 20° of the downwind direction the profiles are blueshifted relative to the star. This is the expected signature of broad heliosheath absorption, and the most downwind directions are where it is expected to be seen, so these three lines of sight can now be considered to represent heliospheric absorption detections, though the manner of detection is very different from the detections depicted in Fig. 1. The θ angle of 160° where the heliosheath absorption starts to become apparent may prove to be a useful diagnostic of the nature of the heliotail.

Figure 3 shows a sky map of the HST-observed lines of sight with Lyα spectra that have been searched for evidence of heliospheric absorption. The boxes are the lines of sight with detections of absorption, while the diamonds and plus signs are nondetections. As noted above, most of the detections are in the upwind direction, but the figure also shows the 3 new detections that are very close to the downwind direction. Even the nondetections can potentially be used to constrain models, as they place limits on the amount of heliospheric absorption that can be present in those directions. The 20 numbered lines of sight scattered around Fig. 3 indicate the sight lines that have been chosen in the past to test models (Wood et al. 2007a). These include the 11 sight lines with detected heliospheric absorption, and 9 sight lines with nondetections chosen to sample directions not covered by the detections.

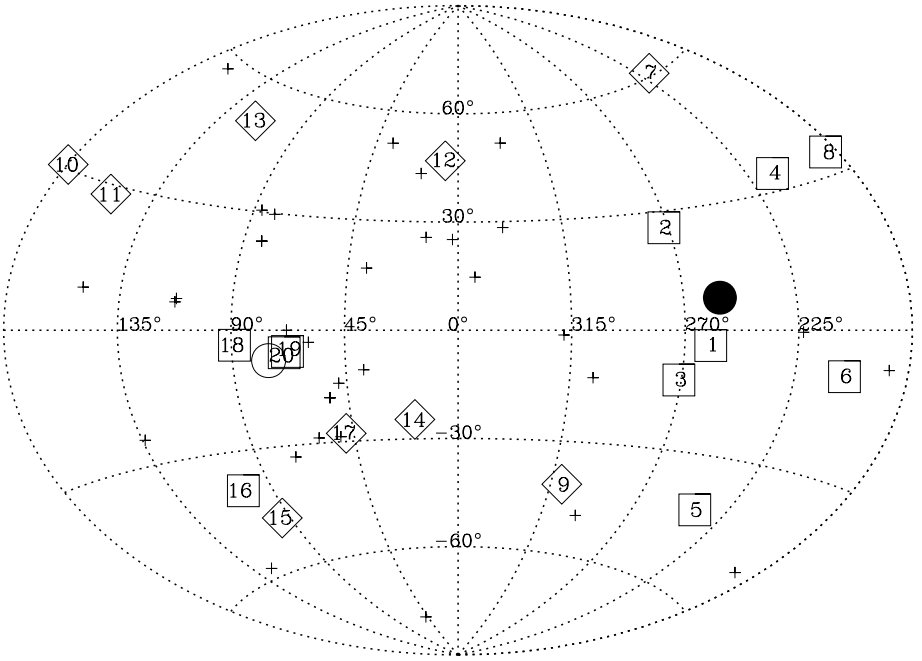

Fig. 3 Sky map in ecliptic coordinates of all HST-observed lines of sight with analyzed Lyα spectra. Numbered symbols indicate spectra that have been used to test model predictions of Lyα absorption (see Figs. 4, 5, and 7). *Boxes* indicate lines of sight with detected heliospheric absorption, while the *diamonds* and *plus signs* are nondetections. The *diamonds* indicate lines of sight with nondetections selected to provide upper limits for absorption in those directions. The *filled* and *open circles* indicate the upwind and downwind directions of the local ISM flow vector, respectively. From Wood et al. (2007a)

3 Absorption Dependence on the ISM Magnetic Field

Evidence for an asymmetric heliosphere has recently been provided by the *Voyager* satellites' observations near the termination shock, and by the different flow vectors measured for interstellar H and He within the solar system (Lallement et al. 2005; Opher et al. 2006; Stone and Richardson 2008). The principle cause of heliospheric asymmetry is expected to be an ISM magnetic field that is skewed with respect to the ISM flow seen by the Sun. The observations have stimulated the development of 3D MHD heliospheric models that can model the observed asymmetries and explore how heliospheric asymmetry depends on ISM field strength and orientation (Izmodenov et al. 2005; Opher et al. 2006; Pogorelov and Zank 2006; Opher et al. 2008; Izmodenov 2008). Some of these models are able to model the neutrals and can also be used to assess what effects the ISM magnetic field should have on the Lyα absorption diagnostic.

Figure 4 compares observed absorption with that predicted by models towards 4 of the lines of sight indicated in Fig. 2 (Wood et al. 2007a). The 3 models assumed different magnetic field strengths: $B = 0$, 1.25, and 2.5 μG. Field strengths higher than this tend to push the termination shock inside the 94 AU distance found by *Voyager 1* (Stone et al. 2005). The orientation of the magnetic field is assumed to be at an angle of $\alpha = 45°$ from the upwind direction of the ISM flow, in the plane suggested for the ISM field by the deflection of H atoms relative to He atoms within the solar system (Lallement et al. 2005). The

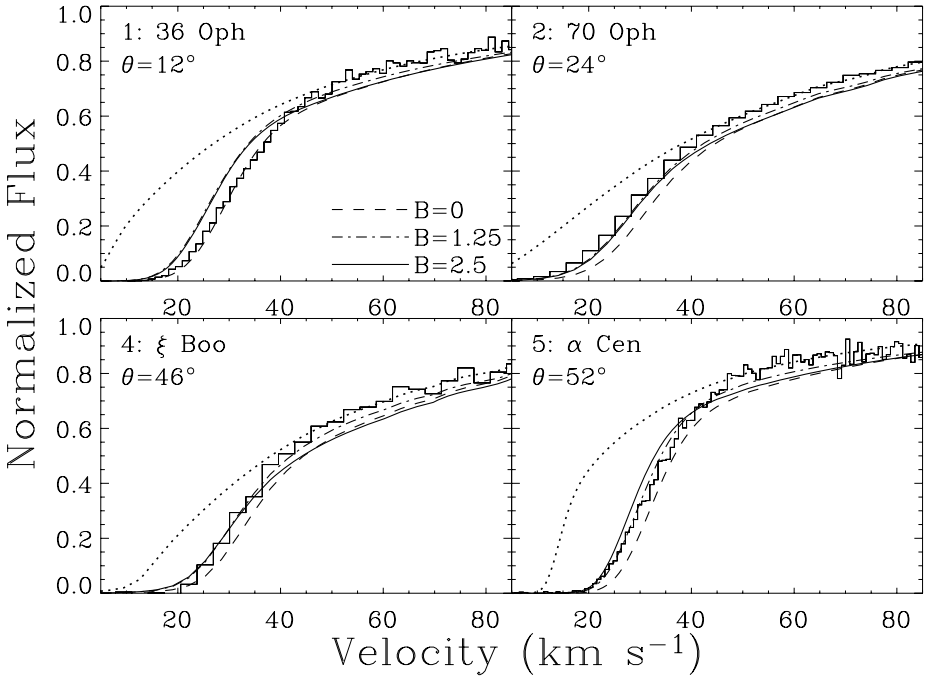

Fig. 4 The red side of the H I Lyα absorption line (histogram) for four stars with detection heliospheric absorption, with the number of the star indicating its location in Fig. 3. The stars are in order of increasing angle from the upwind direction of the ISM flow (θ). In each panel, the *dotted line* is the ISM absorption alone. Absorption predictions are shown for heliospheric models computed assuming ISM magnetic field strengths of 0, 1.25, and 2.5 μG (Wood et al. 2007a)

ISM hydrogen and proton densities assumed in these models are $n_\infty(\mathrm{HI}) = 0.18$ cm^{-3} and $n_\infty(\mathrm{H}^+) = 0.06$ cm^{-3}, the ISM flow speed is $V_\infty = 26.4$ km s^{-1}, and the temperature is $T_\infty = 6400$ K (Izmodenov et al. 2005).

The panels in Fig. 4 show only the redshifted side of the Lyα absorption profiles where the heliospheric absorption will be located. Each panel shows the ISM absorption alone, and the excess absorption from the heliosphere, which the models are attempting to reproduce. Full descriptions of the Lyα data and its analysis can be found in Wood et al. (2005b).

Increasing the magnetic field generally decreases the amount of absorption, though there is little difference in the absorption predicted by the $B = 1.25$ μG and $B = 2.5$ μG models. The decrease is because a higher ISM field weakens the bow shock, leading to lower densities in the hydrogen wall and less absorption, despite the hydrogen wall being somewhat thicker (Wood et al. 2007a). The $B = 1.25$ μG and $B = 2.5$ μG models seem to fit the data particularly well in Fig. 4, though the $B = 0$ μG model works best for the most upwind line of sight (36 Oph). The lines of sight chosen in Fig. 4 are all upwind lines of sight with detected heliospheric absorption. There is little point in comparing the data and model predictions for downwind lines of sight because these particular models do not extend far enough downwind to capture all the absorption in such directions.

Not only does the absorption depend on the strength of the ISM field, it also depends on the orientation of the field. Figure 5 compares the observed absorption with that predicted by various models, for the same 4 lines of sight as in Fig. 4. The models are like the $B = 2.5$ μG model from Fig. 4, but with different α orientation angles. Rather than show the direct

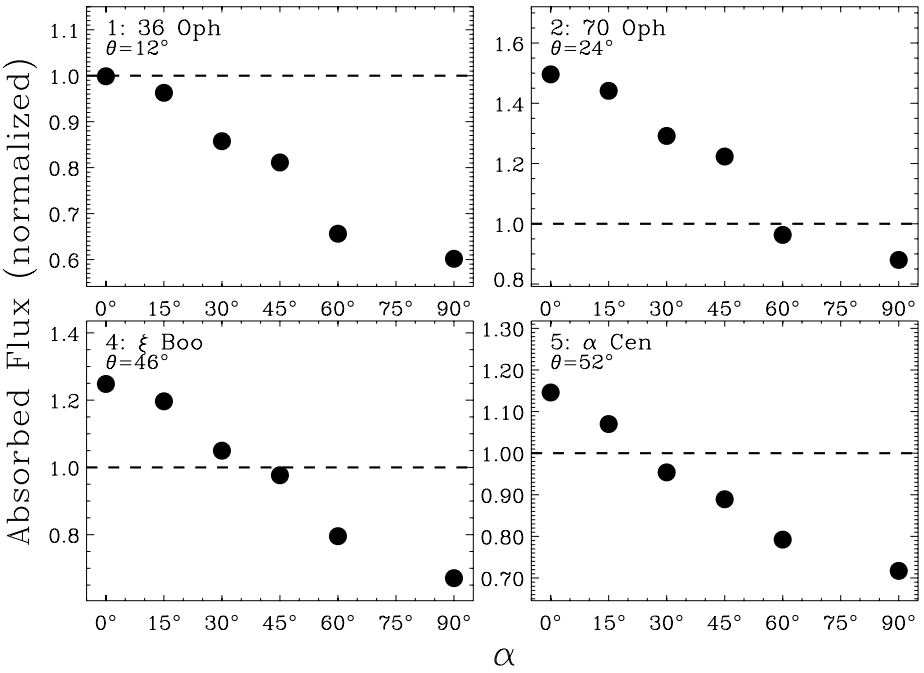

Fig. 5 For the same four upwind lines of sight as in Fig. 4, the predicted wavelength-integrated Lyα flux absorbed by heliospheric H I beyond that absorbed by the ISM is computed for six models with different ISM field orientation, where the α orientation angle is the angle of the field relative to the upwind direction of the ISM flow. The fluxes are normalized to the observed amount of flux absorbed, so in each panel a flux of 1 (*dashed lines*) corresponds to agreement with the data (Wood et al. 2007a)

data/model comparison like in Fig. 4, Fig. 5 computes the absorbed flux predicted by the models divided by the absorbed flux observed in the data, and plots this normalized flux versus α. Absorption decreases with increasing α. There is certainly some scatter in the results, but on average the $\alpha = 15°$–$45°$ models fit the data best, consistent with the $\alpha = 30°$–$60°$ range suggested by Opher et al. (2006) on the basis of termination shock asymmetries observed by the *Voyager* satellites.

For the upwind lines of sight that are the focus of Figs. 4 and 5, the absorption will be dominated by hydrogen wall neutrals. The ISM magnetic field results in a hydrogen wall that is asymmetric, thicker in one hemisphere than the other. However, the models predict that these asymmetries surprisingly do not lead to significant asymmetries in the Lyα absorption. The reason is that densities are lower in parts of the hydrogen wall that are thicker. The hydrogen wall thickness and density effects nearly cancel each other out, and as a consequence there is little azimuthal dependence in the hydrogen wall absorption to act as a signature of heliospheric asymmetries induced by the magnetic field.

However, this is not the case for the heliosheath absorption that dominates in downwind directions. It turns out that unlike the hydrogen wall, the asymmetries in the heliosheath induced by the ISM magnetic field *will* be accompanied by asymmetries in the heliosheath Lyα absorption. But it is only in downwind directions that heliosheath absorption is detectable, and there are only 4 stars with detected absorption in that direction (stars 16 and 18–20 in Fig. 3). This is really not enough to search for azimuthal asymmetries in the absorption that might be diagnostic of the ISM field orientation. Another problem is that most models, in-

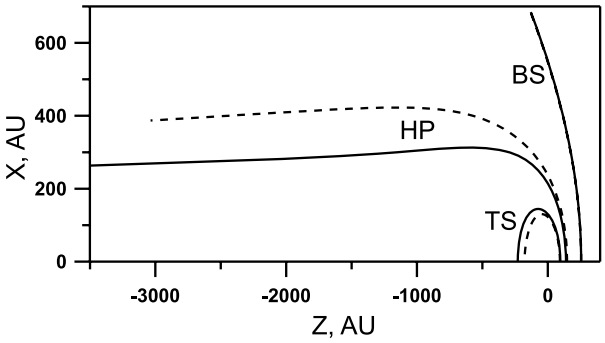

Fig. 6 The locations of the termination shock (TS), heliopause (HP), and bow shock (BS) according to the single-fluid (*dashed lines*) and multi-component (*solid lines*) plasma models (see text for model details). The Sun is at the origin

cluding the ones used in Figs. 4 and 5, do not extend far enough downwind to allow for a comparison between the data and models. Thus, it is not entirely clear from existing models what the extent of the absorption asymmetry should be (Wood et al. 2007a).

4 Extended Tail Models

There are only a few heliospheric models that have been computed that can provide a meaningful data/model absorption comparison for very downwind directions. Such a comparison requires that the model have a proper self-consistent treatment of the neutrals, and the model grid must extend many thousands of AU downwind to be able to capture all the absorption in those directions. Izmodenov and Alexashov (2003) and Alexashov et al. (2004) report on 2-dimensional models of the Baranov and Malama (1993, 1995) type that have been computed with extended tails and a full kinetic treatment of the neutrals. The dashed lines in Fig. 6 show the heliospheric structure of one of these long tail models, with input parameters identical to those of the models in Sect. 3, but with no ISM magnetic field.

The solid lines in Fig. 6 show the heliospheric structure of a model with identical input parameters, but with a much more sophisticated treatment of the plasma in the heliosphere. Although the traditional Baranov and Malama (1993, 1995) type models include a fully kinetic treatment of the neutrals in the heliosphere, they use a single-fluid treatment of the plasma. This is simplistic, however, as the example of pickup protons indicates, which are found not to be thermalized with the ambient solar wind protons within the solar system (e.g., Gloeckler and Geiss 2004). Malama et al. (2006) have modified the Baranov and Malama code to allow for a complex multicomponent treatment of the plasma. The solid lines in Fig. 6 indicate how the multicomponent treatment affects the heliospheric structure predicted by the model. The two models in Fig. 6 are both extended-tail models that can be used to assess whether the multicomponent treatment affects the Lyα absorption predicted by the models. It turns out that the hydrogen wall absorption is completely unchanged. However, the heliosheath absorption that dominates in downwind directions is affected (Wood et al. 2007b).

The model grid for these models extends 5000 AU in the downwind direction. In order to see if this is far enough to capture the absorption towards even the most downwind directions in Fig. 3, we compute the absorption towards these stars using both the full model grid and one that is truncated at shorter distances. At a distance of 3000 AU we see little difference in the absorption, but discrepancies become more significant at shorter truncation distances. Thus, we conclude that modeling the most downwind HST-observed directions requires grids that extend at least 3000 AU downwind.

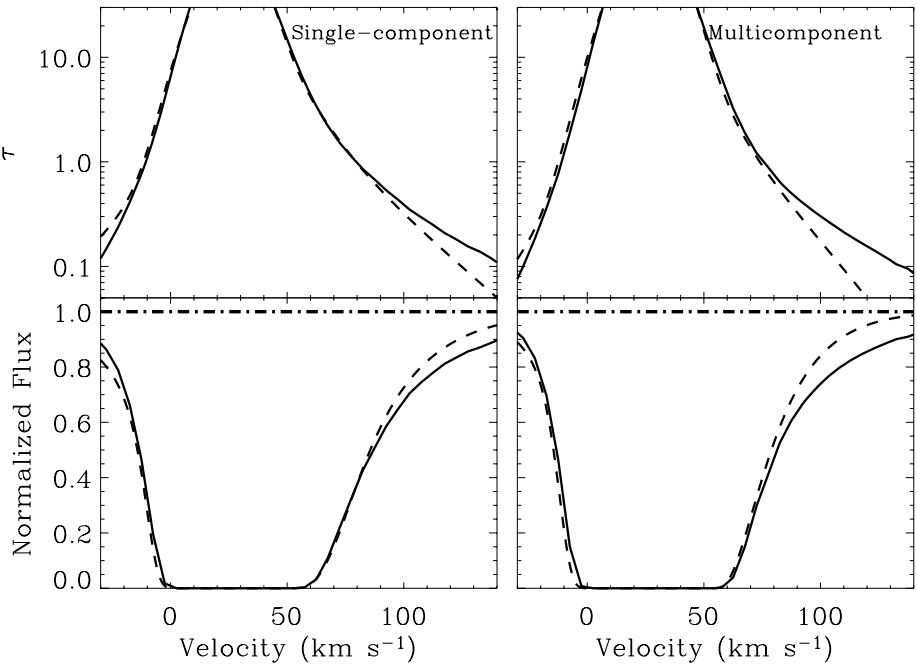

Fig. 7 The *top panels* show the opacity profiles for the absorption towards χ^1 Ori (star #18 from Fig. 3) predicted by the extended-tail single-component and multicomponent models, where the *solid lines* are the exact profiles derived from the kinetic codes and the *dashed lines* are profiles computed using local Maxwellian approximations to the velocity distributions of individual particle components. The *bottom panels* show the absorption profiles that correspond to these opacity functions. There are significant differences, particularly in the red wing of the absorption, emphasizing the inadequacy of the local Maxwellian approximation

The original method used to compute absorption profiles from Baranov and Malama (1993, 1995) style models used local Maxwellian approximations of individual populations of neutrals within the heliosphere (Izmodenov et al. 2002). This may be a good approximation for the hydrogen wall neutrals that dominate the absorption in upwind and sidewind directions, but we find that it does not work well at all for the heliosheath neutrals that dominate in downwind directions. This is shown explicitly in Fig. 7, which compares opacity and absorption profiles computed directly from line-of-sight integrated velocity distributions to ones computed using the local Maxwellian approximations. This is done for a downwind line of sight for both the single-component and multicomponent extended-tail models. There are significant differences, especially in the red wing of the line, which is where the detectable heliosheath absorption lies. Using the local Maxwellian approximation would lead to significant underestimation of heliosheath absorption in the red wing.

Figure 8 shows the absorption predicted by both the single-component and multicomponent models shown in Fig. 6, for four of the downwind lines of sight indicated in Fig. 3 (sight lines 15–19). The Sirius panel of Fig. 8 is analogous to those in Fig. 4, with detected heliospheric absorption. The ϵ Eri panel shows the absorption data for a line of sight with no detected heliospheric absorption. The dashed line in the panel indicates an upper limit for the amount of absorption that can be present while still being consistent with the data. A successful model should predict an absorption profile above the dashed line. The very downwind χ^1 Ori and HD 28205 lines of sight have heliospheric absorption detections, but

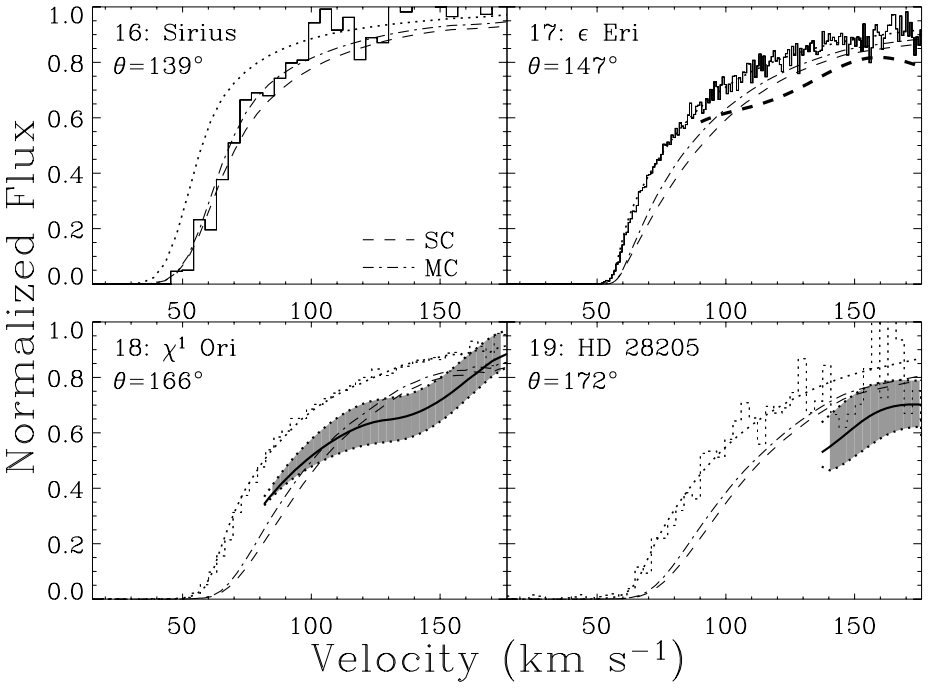

Fig. 8 The red side of the H I Lyα absorption line (histogram) for four of the downwind lines of sight indicated in Fig. 3, with θ indicating the angle from the upwind direction of the ISM flow (θ). The Sirius panel is like those from Fig. 4, with detected heliospheric absorption beyond that from the ISM (the *dotted line*). The ϵ Eri line of sight is a nondetection, where *the thick dashed* line in the panel provides an upper limit for how much absorption a model can predict towards ϵ Eri while still being consistent with the data. Model absorption profiles should lie above that line. The χ^1 Ori and HD 28205 lines of sight are heliospheric absorption detections inferred from line shifts of the reconstructed stellar Lyα profiles. The *shaded regions* in those panels indicate the amount of absorption that models *should* predict if the real stellar Lyα profile is centered on the stellar rest frame. For these lines of sight, the absorption predicted by the models should not fit the data (which are *dotted* histograms in these cases) but should instead fall within the shaded regions. The *dashed* and *dot-dashed lines* are the predicted heliospheric Lyα absorption of models with a single component (SC) plasma and a multi-component (MC) plasma, respectively

only on the basis of the line shift arguments from Sect. 2, and illustrated by Fig. 2. The line shift means that the original reconstructed stellar Lyα profile is inaccurate and the normalized fluxes in Fig. 8 (dashed histograms) are therefore inaccurate. The shaded regions in the figure indicate where the normalized fluxes *should* be if the background stellar profile is forced to be centered on the rest frame of the star. A successful model should predict absorption that lies within these shaded regions for those two lines of sight (Wood et al. 2007a).

The multicomponent model predicts less heliosheath absorption than the single component model. This is due to the overemphasis of the effects of minority high-temperature constituents on the plasma velocity distributions in the simplistic single-component model. The effect is to artificially broaden the distributions, a problem that is then transmitted to the neutral distributions via charge exchange. The reduced absorption of the multicomponent model provides improved agreement with the data for the Sirius and χ^1 Ori lines of sight in Fig. 8. The absorption predicted by the single-component model may be in conflict with the absorption limit towards ϵ Eri near 100 km s^{-1}, but the conflict is lessened for the

multicomponent model. Both models may slightly underestimate the amount of absorption in the most downwind direction (HD 28205).

It is worth noting that the heliosheath neutrals that are responsible for the heliosheath absorption observed and modeled in Fig. 8 are essentially the same population of neutrals that the *Interstellar Boundary Explorer* (IBEX) will observe after it is launched in 2008 (McComas et al. 2005; McComas 2008). The effects that the multicomponent treatment has on the heliosheath absorption, which seems to improve agreement with the data, suggest that the heliosheath particle distributions that IBEX will observe locally may also be better modeled with a multicomponent treatment of heliospheric plasma. Combining IBEX and Lyα absorption constraints on such multicomponent models will be an interesting exercise for the future.

Acknowledgements This work was supported by NASA grant NNG05GD69G to the University of Colorado. V.I. was supported in part by RFBR grants 07-02-01101 and 05-02-22000.

References

D.B. Alexashov, V.V. Izmodenov, S. Grzedzielski, Adv. Space Res. **34**, 109 (2004)
V.B. Baranov, Y.G. Malama, J. Geophys. Res. **98**, 15157 (1993)
V.B. Baranov, Y.G. Malama, J. Geophys. Res. **100**, 14755 (1995)
V.B. Baranov, M.G. Lebedev, Y.G. Malama, Astrophys. J. **375**, 347 (1991)
G. Gloeckler, J. Geiss, Adv. Space Res. **34**, 53 (2004)
V.V. Izmodenov, Space Sci. Rev. (2008, this issue)
V.V. Izmodenov, D.B. Alexashov, Astron. Lett. **29**, 58 (2003)
V.V. Izmodenov, B.E. Wood, R. Lallement, J. Geophys. Res. **107**, 1308 (2002)
V. Izmodenov, D. Alexashov, A. Myasnikov, Astron. Astrophys. **437**, L35 (2005)
R. Lallement, E. Quémerais, J.L. Bertaux, S. Ferron, D. Koutroumpa, R. Pellinen, Science **307**, 1447 (2005)
J.L. Linsky, B.E. Wood, Astrophys. J. **463**, 254 (1996)
Y.G. Malama, V.V. Izmodenov, S.V. Chalov, Astron. Astrophys. **445**, 693 (2006)
D.J. McComas, Space Sci. Rev. (2008, this issue)
D. McComas et al., in *Solar Wind 11/SOHO 16: Connecting the Sun and Heliosphere*, ed. by B. Fleck, T.H. Zurbuchen (ESA, Noordwijk, 2005), p. 689
M. Opher, E.C. Stone, P.C. Liewer, Astrophys. J. **640**, L71 (2006)
M. Opher, E.C. Stone, J.C. Richardson, G. Toth, T. Gombosi, Space Sci. Rev. (2008, this issue)
N.P. Pogorelov, G.P. Zank, Astrophys. J. **636**, L161 (2006)
E.C. Stone, J.C. Richardson, Space Sci. Rev. (2008, this issue)
E.C. Stone, A.C. Cummings, F.B. McDonald, B.C. Heikkila, N. Lal, W.R. Webber, Science **309**, 2017 (2005)
B.E. Wood, H.-R. Müller, G.P. Zank, Astrophys. J. **542**, 493 (2000)
B.E. Wood, H.-R. Müller, G.P. Zank, J.L. Linsky, S. Redfield, Astrophys. J. **628**, L143 (2005a)
B.E. Wood, S. Redfield, J.L. Linsky, H.-R. Müller, G.P. Zank, Astrophys. J. Suppl. Ser. **159**, 118 (2005b)
B.E. Wood, V.V. Izmodenov, J.L. Linsky, D. Alexashov, Astrophys. J. **659**, 1784 (2007a)
B.E. Wood, V.V. Izmodenov, J.L. Linsky, Y.G. Malama, Astrophys. J. **657**, 609 (2007b)